Hydrol. Earth Syst. Sci. Discuss., 8, 6257–6289, 2011
www.hydrol-earth-syst-sci-discuss.net/8/6257/2011/
doi:10.5194/hessd-8-6257-2011

Hydrology and Earth System Sciences Discussions

Heat transport of diurnal temperature oscillations upon river-water infiltration investigated by fiber-optic high-resolution temperature profiling

T. Vogt[1,*], **M. Schirmer**[1], **and O. A. Cirpka**[2]

[1]Eawag – Swiss Federal Institute of Aquatic Science and Technology, Überlandstr. 133, 8600 Dübendorf, Switzerland
[2]University of Tübingen, Center for Applied Geoscience, Sigwartstr. 10, 72076 Tübingen, Germany

[*] *Invited contribution by T. Vogt, recipient of the EGU Young Scientists Outstanding Poster Paper Award 2009.*

Received: 6 June 2011 – Accepted: 18 June 2011 – Published: 29 June 2011

Correspondence to: M. Schirmer (mario.schirmer@eawag.ch)

Published by Copernicus Publications on behalf of the European Geosciences Union.

Abstract

River-water infiltration is of high relevance for hyporheic and riparian groundwater ecology as well as for drinking water supply by river-bank filtration. Heat has become a popular natural tracer to estimate exchange rates between rivers and groundwater. However, quantifying flow patterns and velocities is impeded by spatial and temporal variations of exchange fluxes, insufficient sensors spacing during field investigations, or simplifying assumptions for analysis or modeling such as uniform flow. The objective of this study is to investigate local heat transport upon river-water infiltration in the riverbed and the adjacent riparian zone of the losing River Thur in northeast Switzerland. Here we have applied distributed temperature sensing (DTS) along optical fibers wrapped around three tubes to measure high-resolution temperature profiles of the unsaturated zone and shallow groundwater. Diurnal temperature oscillations were tracked in the subsurface and analyzed by means of dynamic harmonic regression to extract amplitudes and phase angles. Subsequent calculations of amplitude attenuation and time shift relative to the river signal show in detail vertical and temporal variations of heat transport. In addition, we apply a numerical two-dimensional heat transport model for the unsaturated zone and shallow groundwater to get a better understanding of the observed heat transport processes in the riparian zone. Our results show that heat transfer of diurnal temperature oscillations from the losing river through groundwater is influenced by thermal exchange with the unsaturated zone. Neglecting the influence of the unsaturated zone would cause biased interpretation and underestimation of groundwater flow velocities. In addition, the observed riparian groundwater temperature distribution cannot be described by uniform flow, but rather by horizontal groundwater flow velocities varying over depth.

HESSD

8, 6257–6289, 2011

1 Introduction

The biogeochemical and ecological processes at the river – groundwater interface depend on the exchange between both water bodies (Boulton et al., 1998; Hayashi and Rosenberry, 2002). These exchange fluxes include water, solutes, and heat. Quantifying these fluxes including their temporal and spatial variability is crucial for a mechanistic understanding of processes in the hyporheic and riparian zone.

In recent years, temperature fluctuations have increasingly been used as a natural tracer for investigations of hyporheic exchange and groundwater travel times (Fanelli and Lautz, 2008; Goto et al., 2005; Schmidt et al., 2006; Hoehn and Cirpka, 2006; Su et al., 2004). In contrast to artificial tracer tests for the determination of travel times and flow velocities upon bank filtration, the temperature fluctuations of river water offer a natural, continuous varying signal that can be measured in a cost-efficient and robust way. Recently, Anderson (2005) and Constantz (2008) reviewed how heat can be utilized as a tracer for hydrological purposes especially in streambeds, where seepage rates are calculated based on temperature profiles and time series. In this context, quasi-transient analytical solutions of one-dimensional (1-D) heat transport with sinusoidal fluctuations of heat-input on top and constant groundwater temperature at bottom are most commonly applied (Silliman et al., 1995; Stallman, 1965). Based on this approach, several methods of time-series analysis have been developed to calculate time-dependent streambed seepage rates using extracted amplitudes and time shifts of the diurnal temperature signal (Hatch et al., 2006; Keery et al., 2007; Vogt et al., 2010b). Because high-frequency temperature fluctuations are lost due to strong dampening within a few meters of travel distance, the travel time from a losing river to a near-by pumping well may be inferred from the seasonal rather than diurnal temperature signal (Vogt et al., 2009).

Thermal sediment properties needed for the analysis of heat transport in porous media are less variable than hydraulic sediment properties, which is an advantage of heat as tracer over Darcy based methods. However, simplifying assumptions, commonly

HESSD
8, 6257–6289, 2011

made in the analysis of heat as a tracer, may lead to systematic errors in the interpretation. Lautz (2010) showed that non-vertical flow in the riverbed causes the biggest error in 1-D estimates of vertical seepage velocity compared to other non-ideal field conditions, such as a non-sinusoidal signal and a thermal gradient. In addition, uncertainty in thermal diffusivity, sensor spacing, and the accuracy of temperature sensors can cause erroneous predictions of seepage velocities, especially for gaining conditions and low flow velocities (Shanafield et al., 2011). Rau et al. (2010) tested the advantages, limitations and applicability of the methods of Hatch et al. (2006) and Stallman (1965). They hypothesized that analyzing temperature profiles and time series caused by multi-dimensional flow by 1-D solutions may result in inaccurate estimates and that the conditions of a representative elementary volume (REV) needed in the analysis may not be satisfied at the scale of investigation. Molina-Giraldo et al. (2011) demonstrated that conductive heat transfer between shallow aquifers, the underlying aquitard, and the overlaying unsaturated zone may significantly influence transport of seasonal temperature signals through groundwater, and neglecting these impact could cause severe errors in the estimate of groundwater velocities from these signals.

Streambed and groundwater temperature measurements may be performed in observation wells equipped with thermistors or thermocouples included in self-contained data loggers or water-level loggers. An additional lag time should be accounted for sensors not placed in a screened interval due to thermal skin effects (Cardenas, 2010). Rau et al. (2010) separated the screened intervals with thermal insulator discs in the well. Buried sensors without pipes may be deployed in ephemeral streambeds and banks. Vogt et al. (2010b) measured high-resolution temperature profiles along a wrapped optical fiber in direct contact to the riverbed sediments using Raman-scattering based distributed temperature sensing (DTS). In DTS, the optical fiber is the temperature sensor. Laser pulses are injected into and backscattered along the fiber. From the ratio of the temperature independent Stokes and temperature depended anti-Stokes signals, the temperature at the scattering point can be inferred (Selker et al., 2006a). The location of backscatter is computed from the travel time

HESSD
8, 6257–6289, 2011

of the backscattered light. Common commercial DTS devices allow for a spatial resolution of 1 m along an optical fiber of several kilometer length. Integrating over many laser pulses improves the accuracy of the measurement. For hydrological applications, typical measurement time intervals range between 0.5–15 min. Depending on instrument manufacturer and experimental set-up, the temperature resolution varies from 0.01–0.5 K. Suárez et al. (2011) found that DTS systems connected to wrapped optical fibers resolve temperatures with very small variability compared to traditional temperature sensors that may have less noise, but may not reach the high spatial resolution. Besides wrapped optical fibers, DTS has also been used to identify groundwater exfiltration areas from temperature anomalies detected along optical fibers laid out on the river bottom (Lowry et al., 2007). Estimation of groundwater exfiltration rates is possible with simple two-component mixing models (Briggs, 2011; Selker, 2006b) or comprehensive stream heat budget models (Westhoff et al., 2007). In the unsaturated zone, the soil moisture distribution and thermal diffusivity has been estimated based on DTS measurements along buried fiber-optic cables (Steele-Dunne et al., 2010).

The objective of this study is to investigate local heat transport upon river-water infiltration in the streambed and the riparian zone of the losing River Thur in northeast Switzerland. Our main hypothesis is that thermal exchange with the unsaturated zone effects the travel-time distribution of the diurnal temperature signal in shallow riparian groundwater. To test the hypothesis, we use time series of three high-resolution fiber-optic temperature profiles (vertical resolution = 5 mm) to identify spatial patterns of heat transport in the riverbed and the riparian zone upon river-water infiltration. The time-dependent amplitude dampening and time shift of the diurnal signal in the sediments is calculated by means of dynamic harmonic regression (Young et al., 1999). We simulate two-dimensional heat transport in a vertical cross-section covering the saturated and unsaturated zone to demonstrate how transport of diurnal temperature signals within shallow groundwater in the river bank is affected by heat exchange with the unsaturated zone. The latter simulations help understanding the observed temperature time series and exemplify that 1-D interpretation of temperature time series neglecting transverse

HESSD
8, 6257–6289, 2011

heat conduction may lead to a systematic bias in estimated infiltration rates. The latter statement was made by (Molina-Giraldo et al., 2011) for seasonal time series, and is confirmed here for diurnal time series as well.

2 Theory

2.1 Heat transport equation in time and spectral domains

Heat transport in porous media can be described by the convection-conduction equation (Domenico and Schwartz, 2008):

$$\frac{\partial T}{\partial t} + \boldsymbol{v}_T \cdot \nabla T - \nabla \cdot (\mathbf{D}_T \nabla T) = 0 \tag{1}$$

with:

$$\boldsymbol{v}_T = \frac{\rho_w C_w}{\rho_s C_s (1-n) + \rho_w C_w n} \boldsymbol{q}; \mathbf{D}_T = \frac{\lambda_s (1-n)\mathbf{I} + \left(\lambda_w \mathbf{I} + \rho_w C_w \mathbf{D}_{\text{disp}}\right) n}{\rho_s C_s (1-n) + \rho_w C_w n}, \tag{2}$$

in which T denotes temperature (K), t is time (s), $\mathbf{v}_T$ is the effective velocity of convective heat transport ($\mathrm{m\,s^{-1}}$), and $\mathbf{D}_T$ is the effective diffusivity tensor for heat transfer ($\mathrm{m^2\,s^{-1}}$). ρ_w, C_w, and λ_w are the mass density ($\mathrm{kg\,m^{-3}}$), specific heat capacity ($\mathrm{J\,kg^{-1}\,K^{-1}}$), and thermal conductivity ($\mathrm{W\,m^{-1}\,K^{-1}}$) of water. ρ_s, C_s, and λ_s are the corresponding properties of the solids; n denotes porosity; and $\mathbf{I}$ is the identity matrix. The effective thermal velocity depends on $\boldsymbol{q}$, which is the specific discharge vector, and the thermal diffusivity is related to $\mathbf{D}_{\text{disp}}$, which is the hydrodynamic dispersion tensor.

In the following review of analytical results, we assume that the transport coefficients $\boldsymbol{v}_T$ and $\mathbf{D}_T$ are constant, facilitating convenient transformation of the heat-transport equation into the spectral domain. The Fourier transform $\tilde{T}(f,\boldsymbol{x})$ of $T(t,\boldsymbol{x})$ in time is defined as:

$$\tilde{T}(f,\boldsymbol{x}) = \int_{-\infty}^{\infty} T(t,\boldsymbol{x}) \exp(-2\pi i t f) dt, \tag{3}$$

HESSD
8, 6257–6289, 2011

in which f is the frequency (1/day), and i is the imaginary number. Then, the heat-transport Eq. (2) becomes in the spectral domain:

$$2\pi i f \tilde{T} + \boldsymbol{v}_T \cdot \nabla \tilde{T} - \nabla \cdot (\mathbf{D}_T \nabla \tilde{T}) = 0, \tag{4}$$

subject to Fourier-transformed boundary conditions.

2.2 Analytical solution of one-dimensional heat transport equation

The standard model used for the analysis of temperature time series in riverbeds is based on 1-D vertical flow and heat transport with constant coefficients (Stallman, 1965). Here we set a fixed, time-periodic temperature at the bottom of the stream, $z = 0$, and vanishing fluctuations at the limit $z \to \infty$ as boundary conditions:

$$\begin{array}{l} T(z=0,t) = \bar{T}_0 + a_0 \times \cos(2\pi(t - t_0^{\max})f) \\ \lim\limits_{z\to\infty} T(z,t) = \bar{T}_\infty \end{array}, \tag{5}$$

in which T_0 and $\overline{T}_\infty$ are the mean temperatures (K) in the river and the aquifer at infinite distance from the stream bottom, respectively, a_0 is the amplitude (K) of temperature fluctuations in the river, $t^{\max}$ is the time (s) of maximum temperature in the river, and the vertical coordinate z is positive downwards. In the spectral domain, the analytical solution is an exponential function of z with complex exponent. Transformation into the time-domain yields (Stallman, 1965):

$$T(z,t) = \bar{T}_0 + a_0 \times \exp\left(-\frac{z}{z_p}\right) \times \cos\left(2\pi\left(t - t_0^{\max} - \frac{z}{c}\right)f\right), \tag{6}$$

in which c and z_p are the frequency-dependent celerity ($\mathrm{m\,s^{-1}}$) and penetration depth (m) of temperature propagation.

$$c = v_T \sqrt{\frac{1}{2} + \frac{1}{2}\sqrt{1 + \frac{64\pi^2 f^2 \mathbf{D}_T^2}{v_T^4}}}; \tag{7}$$

HESSD
8, 6257–6289, 2011

$$z_p = \frac{2D_T}{c - v_T}. \quad (8)$$

2.3 Dynamic harmonic regression

To extract the diurnal sinusoidal components from the temperature time series, we use dynamic harmonic regression (Young et al., 1999) as presented by Kerry et al. (2007) and Vogt et al. (2010b). This non-stationary extension of Fourier analysis is implemented in the Matlab-based captain toolbox (Taylor et al., 2007). The forward model is similar to the standard spectral representation of the time series:

$$T(t) = a_0(t) + \sum_{i=1}^{n_f} \left(\alpha_i(t) \cos\left(2\pi i \frac{t}{\tau}\right) + \beta_i(t) \sin\left(2\pi i \frac{t}{\tau}\right) \right), \quad (9)$$

in which $a_0(t)$ is the trend, whereas $\alpha_i(t)$ and $\beta_i(t)$ are the sine and cosine contributions of the frequency i/τ, in which τ is the base period (here one day). All time-dependent coefficients are assumed to be auto-correlated in time. For a detailed description of the determination of $\alpha_0(t)$, $\alpha_i(t)$ and $\beta_i(t)$ we refer to Young et al. (1999) and Taylor et al. (2007). From the sine and cosine coefficients $\alpha_i(t)$ and $\beta_i(t)$ the time-dependent amplitude $a_i(t)$ and phase angle $\phi_i(t)$ for frequency i/τ at time t are calculated:

$$a_i(t) = \sqrt{\alpha_i^2(t) + \beta_i^2(t)}; \quad (10)$$

$$\varphi_i(t) = \tan^{-1}\left(\frac{\alpha_i(t)}{\beta_i(t)}\right). \quad (11)$$

We convert the resulting phase angles $\phi(z,t,f)$ of the diurnal signal for each time point t and depth z to a time point of maximum temperature $t^{\max}$:

$$t^{\max}(z,t,f) = -\frac{\varphi(z,t,f)}{2\pi f}. \quad (12)$$

HESSD
8, 6257–6289, 2011

Then, the time shift $t_{\text{shift}}(z,t,f)$ between the diurnal river and groundwater signals is iteratively calculated by:

$$t_{\text{shift}}(z,t,f) = t^{\max}(z,t,f) - t^{\max}(0,t - t_{\text{shift}}(z,t,f),f). \quad (13)$$

In addition, we compute the attenuation of the diurnal river temperature signal $A(z,t,f)$ during transport through the riverbed to the riparian zone at each time point t and depth z:

$$A(z,t,f) = \ln\left(\frac{a_i^{\text{river}}(t - t_{\text{shift}}(z,t,f),f)}{a_i(z,t,f)}\right). \quad (14)$$

For a time-constant observation depth z we determine the apparent effective velocity $v_T(z,t,f)$ and the apparent effective diffusivity $\mathbf{D}_T(z,t,f)$ of temperature transport after Vogt et al. (2010b) based on the attenuation $A(z,t,f)$ and the apparent celerity $c(z,t,f)$ of the diurnal temperature signal:

$$c(z,t,f) = \frac{z}{t_{\text{shift}}(z,t,f)}, \quad (15)$$

$$W(v_T,\mathbf{D}_T) = \left(1 - \frac{v_T}{c}\sqrt{\frac{1}{2} + \frac{1}{2}\sqrt{1 + \frac{64\pi^2 f^2 \mathbf{D}_T^2}{v_T^4}}}\right)^2 + \left(1 - \frac{2A\mathbf{D}_T}{(c - v_T)z}\right)^2, \quad (16)$$

in which we have dropped the argument (z,t,f) for convenience. Thereto, the sum of the squared relative residuals of $c(v_T,\mathbf{D}_T,f)$ and $z_p(v_T,\mathbf{D}_T,f)$ is minimized and optimization is done by the Nelder-Mead simplex algorithm that is implemented in the Matlab function fminsearch (Lagarias et al., 1998). Finally, the apparent seepage rate $q(z,t)$ related to the diurnal temperature signal (f=1/day) is estimated, if z is constant over time:

$$q(z,t) = v_T(z,t,f)\frac{\rho_s C_s(1-n) + \rho_w C_w n}{\rho_w C_w}. \quad (17)$$

HESSD
8, 6257–6289, 2011

3 Field site

The field site is situated in northeast Switzerland at the western end of the Thur catchment, which is draining the front ranges of the Swiss NE Limestone Alps (Alpstein) into River Rhine (Fig. 1). River Thur exhibits fluctuations in discharge and water table similar to unregulated alpine rivers (low discharge (NQ) 2.2 $m^3 s^{-1}$, mean discharge (MQ) 47 $m^3 s^{-1}$, peaks (HHQ) up to 1130 $m^3 s^{-1}$, HHQ/MQ ratio = 24; BAFU, 2010). Snowmelt and strong rain events in the headwaters cause short but rapid increases of discharge. Mean annual precipitation of the field site area is 908 mm and average monthly temperatures range from 0.9 °C in January to 19.0 °C in July (https://gate.meteoswiss.ch/idaweb).

The aquifer in the Thur valley consists of Pleistocene glacio-fluvial sandy gravels overlaying impervious lacustrine clays. Alluvial fines of up to 2 m thickness act as a confining layer on top of the aquifer, which is 5–7 m thick and has a hydraulic conductivity of $\approx 3 \times 10^{-3}$ $m s^{-1}$ (Schneider et al., 2011). The riverbed consists of sandy gravel and is hydraulically well connected to the aquifer. At the field site, the major groundwater recharge originates from continuous river-water infiltration into the aquifer (Vogt et al., 2010a). The infiltration velocity in the restored riverbed was estimated to fluctuate in the range of 1.5×10^{-5} $m s^{-1}$ to 4.5×10^{-5} $m s^{-1}$ (Vogt et al., 2010b).

The field site is located at a restored section of River Thur and has been detailed investigated by the RECORD project (Assessment and Modeling of Coupled Ecological and Hydrological Dynamics in the Restored Corridor of a River (Restored Corridor Dynamics; http://www.cces.ethz.ch/projects/nature/Record)). Here, the restored riverbed is 60–100 m wide and shows distinct riverbed morphology. The northern bank stabilization has been removed resulting in a riparian zone with a natural succession of bare gravel, grass colonized gravel, willow belt and alluvial forest. Field installations consist of a river gauging station, observation wells with integrated water-level, temperature, and electrical conductivity sensors, meteorological stations and soil sensors, among others (Schneider et al., 2011).

HESSD
8, 6257–6289, 2011

4 Methods

4.1 Fiber-optic high-resolution temperature profiling

We used three high-resolution fiber-optic temperature profilers based on the experimental set-up of (Vogt et al., 2010b), consisting of a solid 2 inch PVC tube (OD = 60 mm) of 2 m length and between 377 and 383 m optical fiber (OD = 0.9 mm) (Fig. 2). Wrapping the fiber around the tube, converts the spatial resolution of the DTS from 1 m along the fiber to a vertical resolution of about 5 mm (±0.1 mm, for the conversion the variability of wrapping must be known) along the 1.92 to 1.93 m long wrapped section. The optical fiber used for wrapping (Dätwyler GF-100) has a multimode glass core with a critical bending radius of 25 mm and is protected by a flexible cladding and coating. Due to the strong variability of river-stage, the DTS control unit was placed elevated 40 m away from the shoreline. We used a four-channel Agilent N4386 DTS system to measure the temperature along the optical fiber operating with 1 m spatial resolution and single-ended measurements. Each of the three fiber-optic high-resolution temperature profilers was connected to one channel of the DTS system and measured consecutively for 30 s averaged to 15 min measurement intervals in a sequence measurement mode. The theoretical temperature resolution is 0.11 K for a 2 km long fiber, 10 min integration time, and 1.5 m spatial resolution in single ended measuring mode (according to technical datasheet of manufacturer, AP Sensing GmbH, 2009). Connection of each wrapped fiber-optic cable to the DTS system was made by a steel-protected fiber-optic cable (Drahtex Arma Fiber) of which 5–10 m were stored in a box filled with a water-ice mixture for calibration. We monitored the temperature in the ice bath, the river water and air temperature with Onset TidbiT v2 sensors (0.02 K resolution, 0.2 K accuracy.). The DTS data of each wrapped optical fiber showed a different temperature offset and systematic drift and were corrected by comparison with the TidBit data.

For field installation of the fiber-optic high-resolution temperature profilers we used a direct-push machine that pushed 3.25 inch metal rods with an expandable tip into the

HESSD
8, 6257–6289, 2011

sediments. The wrapped tubes fit into the metal rods (ID = 67 mm) of the direct-push system and remain with the expendable tip in the ground after pulling the outer metal rod. We installed the three high-resolution temperature profilers in the riverbed, at the shoreline, and in the riparian bank along a presumed subsurface flow path (Fig. 2). The investigated area is about 40 m upstream of the experiment of Vogt et al. (2010b) on the northern side of the restored river section. Here, the riverbed has an elevation of 371.8 m a.sl. and the elevation of the bank is about 372.3 m a.s.l. (Fig. 2). The installation depth of the lower end of the wrapped fibers was 370.5 m a.s.l., but the number of measuring points in air, river-water, saturated and unsaturated zone varied depending on the location and on water-level (Fig. 2). The presented data were acquired during 22 days in September 2010.

4.2 Numerical heat-transport model

We applied a 2-D spectral finite element model of heat transport after Molina-Giraldo et al. (2011) to simulate heat transport within a vertical cross section mimicking the conditions at the experimental site. The model accounts for conductive/dispersive and convective heat transfer in a steady-state groundwater flow field, conductive heat transfer through the unsaturated zone on top, and diurnal temperature fluctuations in the riverbed at the shoreline as well as at the land surface of the river bank (Fig. 3).

The model consists of two layers representing the unsaturated and saturated zone of the riparian zone. The thickness of the unsaturated zone is set to 0.5 m and that of the aquifer to 1 m according to the experimental set-up of the high-resolution temperature profiler in the bank (see Fig. 2). The horizontal extension of the model domain is 10 m. The uniform grid has a vertical resolution of 0.01 m and a horizontal resolution of 0.02 m. A no-flow boundary condition is applied to the bottom of the domain. The water enters the aquifer on the left side with horizontal flow and leaves the aquifer through the right side. We start with a uniform velocity distribution over the entire aquifer thickness. However, velocities can be adjusted to obtain horizontal groundwater flow velocities varying over depth.

HESSD
8, 6257–6289, 2011

At the land surface the temperature oscillations are simulated by a frequency of 1/day and a constant amplitude of 6 K, which is shifted from the river signal as observed at the bank temperature profiler. At the left-hand boundary of the groundwater layer we used amplitude and time-shift profiles of the high-resolution temperature profiler installed at the shoreline from 22 September 2010, 00:08 UTC +2 h as boundary condition. The data were converted into temperature fluctuations. For the unsaturated part of the left- and right-hand boundaries and for the bottom boundary, we assumed zero heat flux. Heat flux at the right aquifer boundary is restricted to convection. The thermal and hydraulic parameters used in the model are literature values typical for sandy gravel sediments consisting of a quartz-calcite mixture (Table 1).

The model simulates the 2-D distribution of Fourier transformed temperature fluctuations $\tilde{T}(f, \boldsymbol{x})$. The amplitude a_T (K) and phase shift ϕ_T (s) of the simulated diurnal temperature signal is then given by:

$$a_T = \left\| \tilde{T} \right\|; \tag{18}$$

$$\varphi_T = \tan^{-1} \left| \frac{Re(\tilde{T})}{Im(\tilde{T})} \right|, \tag{19}$$

which can further be transformed to a time-shift of the temperature maximum according to Eqs. (12) and (13).

5 Results

5.1 Temperature distribution

During the monitoring period, the river water had a mean temperature of 14.6 °C with diurnal amplitudes of 0.4–2.3 °C. The mean air temperature was identical, but diurnal amplitudes were in average 2.3 times higher. Throughout the measurement campaign several minor storm events occurred resulting in higher river stage (at 2, 9, and

HESSD
8, 6257–6289, 2011

13 September 2010). We stopped monitoring on September 25 when a big storm event followed by a major flood occurred. Although the experimental set-up was designed for temporary use, the installations were fully operational after major flood events. Manual measurements of the water table at the three profilers agree well with extrapolated water level data of a well close to the river, where a pressure sensor was installed.

The temperature data of the fiber-optic high-resolution temperature profiler in the riverbed were analyzed after Vogt et al. (2010b). The calculated seepage rates range between 0.8–3.0 $\times 10^{-5}$ m s^{-1} and agree well with the results of Vogt et al. (2010b). In the following, we focus on the shoreline and the bank where an unsaturated zone exists and horizontal flow is dominant.

The upper part of the high-resolution fiber-optic temperature profiler at the shoreline lay above the sediments and the rest in the sandy gravel sediments (Fig. 4a). In contrast to the profiler in the riverbed, at the shoreline an unsaturated zone of up to 0.15 m existed under low flow conditions. During higher river stage, the sediments were flooded. A sharp temperature contrast illustrates the interfaces between air and river water as well as air and sediments (Fig. 4a). The high-resolution fiber-optic temperature profiler in the bank had only a small wrapped section exposed to the air. Figure 4b shows the temperature data of the wrapped optical fiber which was installed in the bank sediments. Here, the top sediment layer consists of silty fine sand with a thickness of about 0.2 m overlaying the sandy-gravel aquifer. Until the end of the monitoring campaign, when the major flood occurred, a varying unsaturated zone of 0.25–0.60 m existed.

All DTS data show noise ranging from 0.02–0.2 K. In the deepest 0.2–0.3 m of the 1.93 m long wrapped section the DTS noise exceeded the very small diurnal temperature oscillations (amplitudes < 0.05 K). Therefore, we focus on the temperature distribution from above 370.7 m a.s.l. to the land surface. The data of the high-resolution temperature profilers reveal in detail the temperature distribution in the riverbed and the riparian zone over depth and time. The top sediments are characterized by strong oscillations, especially when an unsaturated zone exists, whereas the lower groundwater

HESSD
8, 6257–6289, 2011

shows only low diurnal temperature oscillations. The heat signal at the land surface propagates into the unsaturated zone. If the distance to water table is low, like at the shoreline, the maximum penetration depth lies below the water table. The strong decrease of amplitudes and increase of time shift with depth are clearly visible in Fig. 4. In groundwater, the temperature pattern changes to slightly curved features that disappear below 370.7 m a.s.l. The signals of river and land surface temperature interfere at the shoreline in shallow groundwater, whereas the middle and deeper groundwater temperatures are apparently determined by the river signal only (Fig. 4c). In the riparian bank the signal of the land surface is strongly damped in the top sediments and almost disappears before reaching the groundwater table. The earlier occurrence of the temperature maximum is obvious in the middle part of groundwater compared to shallow and deeper groundwater (Fig. 4d).In the bank the temperature distribution at the saturated-unsaturated interface indicates conductive heat exchange between groundwater and unsaturated zone, too. Due to the high resolution, the temporal and spatial variability of the penetration depths of the river and land surface signals as well as their interference is visible in the temperature distributions.

5.2 Results of dynamic harmonic regression analysis

The temperature time series of each 5 mm depth interval are analyzed by dynamic harmonic regression for the frequency 1/day. The elevation of the land surface was stable during the monitoring period. Therefore, the depth z is known and constant over time. According to Eqs. (13) and (14) we use the output of the dynamic harmonic regression, namely the amplitudes and phase angles, to calculate the amplitude attenuation and time shift of the diurnal signal in the unsaturated zone and groundwater related to the river temperature. We investigate only time shift and amplitude attenuation as characteristic parameters for heat transport, because the exact flow path and infiltration point are unknown and therefore the travel distance. When the top sediments vary between flooded and dry, like at the shoreline, the flow direction is changing from vertical to horizontal. Hence, 1-D analytical solutions cannot be applied.

HESSD
8, 6257–6289, 2011

The resulting spatiotemporal distribution of the estimated time shifts for the high-resolution fiber-optic temperature profiler at the shoreline and in the bank is shown in Fig. 5a–b. The diurnal air temperature signal at the top of the sediments has an average time shift of −1.75 h compared to the river temperature. In the shallow sediments the time shift increases almost linearly with depth, especially in the bank where an unsaturated zone continuously exists. The time shift at the shoreline reaches a first maximum of up to 5–6 h in the depth of 371.4–371.6 m a.s.l. and in the bank in 371.6–371.8 m a.s.l. a maximum of up to 11–12 h. Within the next 0.2–0.4 m below the maximum, the time shift decreases and then starts to increase again (Fig. 5c). In the bank, the upper time shift maximum is at the interface between unsaturated and saturated zone. However, the upper time shift maximum at the shoreline lies below the water table. At the beginning of the monitoring period, a bad signal-noise ratio causes negative time shifts in groundwater at the shoreline. The spatiotemporal distribution of the amplitude attenuation shows nearly the same pattern (Fig. 5d). The unsaturated zone is characterized by an almost linear increase in amplitude attenuation and groundwater by high amplitude attenuation in the shallow part, then the attenuation decreases and in the deeper part increases again. In contrast to the time shift, at the unsaturated – saturated interface a stronger increase of amplitude attenuation occurs, although the upper maximum of attenuation lies below the water table, too.

Besides the vertical variability, a pronounced temporal variability of heat transport exists. The special spatial patterns of increasing, decreasing, and again increasing time shifts with depth are present also under different hydrological conditions. At the shoreline, the time shift distribution is patchy with shortest values when the sediments are flooded. Also in the bank the shortest time shifts occur when the water table is high, but here the locations of maximum and minimum time shifts are more stable. While the time-shift distribution is constant in the unsaturated zone, groundwater exhibits the strongest temporal variations (Fig. 5c–d). In the riparian groundwater of the bank at 371.3 m a.s.l. the time shift ranges from 2 h for high and 8 h for low water table. Furthermore, the amplitude attenuation is up to 3–4 times higher at low water table

HESSD
8, 6257–6289, 2011

conditions.

5.3 Model results

Figure 6a and c show the spatial distribution of the diurnal temperature amplitude and time shift as simulated by the 2-D heat transport model. First, the simulations were run with uniform horizontal groundwater velocities. Then we applied depth varying horizontal groundwater flow velocities to get a better agreement between modeled and observed time shifts in riparian groundwater. The applied horizontal velocities are sinusoidally distributed over depth with a minimum of $0.58 \times 10^{-4}\,\mathrm{m\,s^{-1}}$ in 0.7 and 1.4 m depth and fastest velocities with $1.04 \times 10^{-4}\,\mathrm{m\,s^{-1}}$ in the middle part of the aquifer in 0.9–1.0 m depth. The presented amplitudes and time shifts are the simulation results for the depth varying horizontal flow velocities.

The temperature signal originating from the land surface strongly decreases in the top sediments of the unsaturated zone over the entire width of the model domain shown by the strong decrease in amplitudes (Fig. 6a). Below, horizontal differences occur. The amplitudes at the left side in the deeper part of the unsaturated zone become higher closer to the water table, whereas the amplitudes are decreasing with depth in the unsaturated zone on the right side. Compared to the unsaturated zone the amplitudes in the groundwater layer are smaller with a maximum of 2.5 K in shallow groundwater close to the left heat input boundary. Amplitudes are decreasing with depth in the deeper part of the groundwater layer. With increasing distance from the river the amplitude maximum moves continuously deeper below the groundwater table. For illustration, Fig. 6b (black solid line) shows a vertical amplitude profile at 2.5 m distance to the river. This is the distance to the river of the fiber-optic high-resolution temperature profiler installed in the bank whose observed amplitudes from 22 September 2010, 00:08 UTC +2 h are shown, too. In the upper part of the unsaturated zone the data agree very well, but with increasing depth small differences occur.

Figure 6c shows the time-shift distribution of the diurnal signal with respect to the river signal. In the upper part of the unsaturated zone, the time shift increases linear

HESSD
8, 6257–6289, 2011

with depth. The time-shift distribution in the deeper part of the unsaturated zone and the groundwater layer is more complex, because the values show a vertical variability with first decreasing and then again increasing values with depth. In flow direction from left to right the time shift is increasing in the groundwater layer. The zone of high vertical time-shift gradients in the deeper part of the unsaturated zone is moving closer to the water table with increasing distance from the river. Figure 6d shows vertical time-shift profiles to illustrate the vertical time-shift variability at 2.5 m distance to the river and to compare the simulated (black solid line) with the observed (black dashed line) time shift of the fiber-optic high-resolution temperature profiler installed in the bank from 22 September 2010, 00:08 UTC + 2 h. The model reproduces the general trend of linear increase with depth in the unsaturated zone and vertical time-shift variations in groundwater. But the vertical variations of the measured groundwater data are stronger. Moreover, in the simulation the first time-shift maximum lies above water table, whereas in the bank of the riverbed the time shift maximum has almost the same elevation as the water table. At the bottom of the aquifer the simulated and measured time shifts agree well with the measured data.

We demonstrate the effect of depth varying horizontal groundwater flow velocities and heat exchange with the unsaturated zone on the time-shift distribution in Fig. 6d. The grey solid line shows that uniform horizontal groundwater flow velocity fails to explain the observed shortest travel times in the middle groundwater, although time shifts in shallow and deep groundwater are well reproduced. Simulating heat transport in groundwater without thermal exchange with the unsaturated zone (grey dashed line) results in a time-shift profile of short time shifts in shallow groundwater and higher time shifts in deep groundwater, reflecting the vertical differences of travel time at the left model boundary based on the data of the high-resolution temperature profiler at the shoreline. While in deep groundwater no differences between the different models exist, thermal exchange with the unsaturated zone has a big impact on shallow groundwater temperature. Compared to the unaffected time-shift profile (grey dashed line), thermal exchange with the unsaturated zone causes a retardation in shallow

HESSD
8, 6257–6289, 2011

groundwater. In addition, the shortest travel times in the middle groundwater can only be explained by a zone of higher flow velocities.

6 Discussion and conclusions

Quantifying patterns and velocities of heat exchange fluxes between rivers and groundwater is challenging due to temporal and spatial variations. In addition, field investigations are often limited by insufficient sensors spacing and their analysis by simplifying assumptions. The focus of the present study is on a detailed local survey of heat transport upon river water infiltration. The experimental set-up using wrapped optical fibers to monitor high-resolution temperature profiles in the riverbed and the bank is based on the study of Vogt et al. (2010b). In contrast to the latter, our interest lies on the effect of thermal exchange with the unsaturated zone on the time-shift distribution of diurnal temperature fluctuations in hyporheic and riparian groundwater as well as on depth varying horizontal flow velocities in riparian groundwater. To simulate heat transport of the diurnal temperature signal, we have applied the numerical heat-transport model of Molina-Giraldo et al. (2011), which was originally developed to analyze the propagation of seasonal temperature signals.

Our results show that thermal exchange with the unsaturated zone affects the distribution of the diurnal temperature signal in hyporheic and riparian groundwater. Two different heat transport processes and two different heat input sources interact, resulting in a complex temperature field. Heat conduction causes the propagation of the diurnal land-surface temperature signal into the upper part of the unsaturated zone. The strong attenuation of this signal in the upper part of the unsaturated zone can be explained by pure conduction without recharge or infiltration in the unsaturated zone. Above the groundwater table the amplitudes are too high for resulting only from conductive heat propagation from the land surface. Therefore, the temperature signal of shallow groundwater is propagating by heat conduction into the deeper part of the overlying unsaturated zone. The influence of conductive heat transport from groundwater into

HESSD
8, 6257–6289, 2011

the unsaturated zone is decreasing with increasing distance to the river. Convective-conductive heat transport causes the propagation of the river temperature signal into the aquifer. Given a shallow unsaturated zone, which is typical for restored river banks, the two different diurnal temperature signals interfere within the transition zone of the unsaturated zone and groundwater, if the land-surface signal propagates deep enough, or the shallow diurnal groundwater temperature signal is retarded due to conductive heat exchange into the unsaturated zone affecting both amplitude and time shift of the diurnal temperature signal, if the land-surface signal propagates only into the top unsaturated sediments. Even without heat input at the land surface, the conductive exchange with the unsaturated zone results in a retardation of the time shift in shallow groundwater. Molina-Giraldo et al. (2011) simulated the same effect for the seasonal temperature signal considering distances to the river of more than 50 m. They also had to account for heat exchange with the underlying aquitard. The latter was not needed in the present study, because dampening of diurnal temperature fluctuations is much stronger than for seasonal ones, which also explains the shorter travel distances over which the diurnal fluctuations can be observed.

For investigations of river-water infiltration in the hyporheic and riparian zone, the diurnal temperature signal is usually used. In this case, neglecting thermal exchange with the unsaturated zone may cause a biased interpretation of shallow groundwater travel times close to a losing river, resulting in underestimated exchange fluxes. Additional misinterpretations of time shift by multiples of 1 d can occur, if the time until the diurnal signal is totally damped is longer than one day.

The fiber-optic high-resolution monitoring of the spatiotemporal varying temperature field enables detailed insights into the temporal and vertical dynamics of heat transport upon river-water infiltration. Changing river stages cause temporal variability of heat transport: in our investigations, we have observed the shortest time shifts und smallest amplitude attenuation in groundwater during high river stage. In this situation, the hydraulic gradient between river and groundwater is higher, resulting in faster flow and therewith faster heat transport. Of course, the variability of velocity in response to

HESSD
8, 6257–6289, 2011

variations in river stage depends highly on local conditions, e.g. in the study of Cirpka et al. (2007) at a different River-Thur site the groundwater table quickly followed the river stage, so that velocity fluctuations were less pronounced.

The numerical heat transport model has qualitatively reproduced the vertical variability of temperature amplitudes and time shifts within the river bank. In particular, the s-shaped vertical profile of groundwater temperature time shift could be attributed to two different factors. One is the retardation of the temperature signal in shallow groundwater due to heat exchange into the unsaturated zone and the other is vertical variation of the horizontal groundwater flow velocities. The vertical distribution of flow velocities with twice as high velocities in the middle part compared to the shallow and deep part of the groundwater is an important information for future studies on biogeochemical processes upon river water infiltration at the test site and shows the variability of groundwater flow velocities in fluvial sediments close to losing rivers. The model, however, was set up for a single representative flow regime and does not exactly reproduce the spatiotemporal temperature distribution.

The diurnal temperature signal is strongly damped by thermal conduction. The penetration length depends on the thermal diffusivity, flow velocity, and the signal frequency. Therefore, the seasonal temperature signal has a higher penetration distance in both groundwater and the unsaturated zone in comparison to the diurnal signal.

Uncertainty and error sources of our field study are related to sensor resolution as for investigations with standard temperature sensors, too. The time resolution of 15 min intervals was sufficient to monitor the diurnal temperature signal. In contrast to point measurements or sensor-chains with a sensor-depth uncertainty of up to 0.02 m, we know the exact depth and sensor spacing of the wrapped optical fiber. Although the depth intervals were constant over time, possible changes of the land-surface elevation at the installation locations could be observed due to a sharp temperature contrast and the high vertical resolution of the wrapped optical fiber. The high vertical resolution of the fiber-optic profilers and thus the detailed detection of vertical differences of heat transport are their main advantages. Interpretation of the complex temperature

HESSD
8, 6257–6289, 2011

patterns remains vague, if a single point sensor or a chain of point sensors is applied. Conversely, compared to standard temperature sensors with a resolution of 0.02 K, DTS data are noisier. DTS noise can be attributed to the experimental set up namely the instrument's sampling resolution/spatial resolution algorithm (Tyler et al., 2009), white and flicker noise (Suárez et al., 2011), or altering splice connections between the wrapped fiber and the robust connection cable. DTS noise and precision can be improved by increasing the spatial resolution and measurement time interval or by manually calibrating temperatures along the optical fiber as presented by Suárez et al. (2011). If the amplitude of the diurnal signal is lower than the accuracy and noise of the measurement, like below 370.7 m a.s.l. at our field site, the extraction of amplitude and phase angle becomes erroneous. In general, the exact extraction of amplitudes and phase angles by means of dynamic harmonic regression is important. During sunny days, solar radiation caused warming of the fiber-optic cables exposed to air and very shallow river water as reported by Vogt et al. (2010b). However, the impact of solar radiation is similar for standard temperature sensors (Neilson et al., 2010).

Overall, we recommend high-resolution temperature profilers for investigations of heat transport in the hyporheic and riparian zone. To this end, DTS measurements along wrapped optical fibers offer a qualified method. Our field and modeling studies demonstrate the need for accounting thermal exchange of groundwater with the unsaturated zone when using time-shift or amplitude attenuation of the diurnal temperature signal for calculation of flow velocities.

Acknowledgements. This study was financed by the Competence Center Environment and Sustainability (CCES) of the ETH domain in the framework of the RECORD project (Assessment and Modeling of Coupled Ecological and Hydrological Dynamics in the Restored Corridor of a River (Restored Corridor Dynamics)). In addition, this work was supported by the Swiss National Science Foundation (SNF grant 200021–129735 "Alpine Hydrogeology"). We thank Andreas Raffainer and Peter Gäumann of the Eawag workshop for their help in wrapping and installing the fiber-optic temperature profilers.

HESSD
8, 6257–6289, 2011

References

Anderson, M. P.: Heat as a ground water tracer, Ground Water, 43, 951–968, doi:10.1111/j.1745-6584.2005.00052.x, 2005.

BAFU: Hydrologischer Atlas der Schweiz, Bundesamt für Umwelt, Bern, Switzerland, 2010.

Boulton, A. J., Findlay, S., Marmonier, P., Stanley, E. H., and Valett, H. M.: The functional significance of the hyporheic zone in streams and rivers, in: Annual Review of Ecology and Systematics, edited by: Fautin, D. G., Annual Review of Ecology and Systematics: 29, Annual Reviews Inc. {a}, 59–81, 1998.

Briggs, M., Lautz, L., and McKenzie, J.: A comparison of distributed temperature sensing to traditional methods of evaluating groundwater inflow to streams, Hydrol. Process., in review, 2011.

Cardenas, M. B.: Thermal skin effect of pipes in streambeds and its implications on groundwater flux estimation using diurnal temperature signals, Water Resour. Res., 46, W03536, doi:10.1029/2009wr008528, 2010.

Carsel, R. and Parrish, R.: Developing joint probability distributions of soil water retention characteristics, Water Resour. Res., 24, 755–769, 1988.

Cirpka, O. A., Fienen, M. N., Hofer, M., Hoehn, E., Tessarini, A., Kipfer, R., and Kitanidis, P. K.: Analyzing bank filtration by deconvoluting time series of electric conductivity, Ground Water, 45, 318–328, 2007.

Constantz, J.: Heat as a tracer to determine streambed water exchanges, Water Resour. Res., 44, W00D10, doi:10.1029/2008WR006996, 2008.

de Marsily, G.: Quantitative Hydrogeology, Academic Press, San Diego, California, 1986.

Domenico, P. A. and Schwartz, F. W.: Physical and chemical hydrogeology, John Wiley & Sons Inc., New York, 528 pp., 2008.

Fanelli, R. M. and Lautz, L. K.: Patterns of water, heat, and solute flux through streambeds around small dams, Ground Water, 46, 671–687, doi:10.1111/j.1745-6584.2008.00461.x, 2008.

Goto, S., Yamano, M., and Kinoshita, M.: Thermal response of sediment with vertical fluid flow to periodic temperature variation at the surface, J. Geophys. Res.-Sol. Ea., 110(11), B01106, doi:10.1029/2004jb003419, 2005.

Hatch, C. E., Fisher, A. T., Revenaugh, J. S., Constantz, J., and Ruehl, C.: Quantifying surface water-groundwater interactions using time series analysis of streambed thermal records:

HESSD
8, 6257–6289, 2011

Method development, Water Resour. Res., 42(14), W10410, doi:10.1029/2005wr004787, 2006.
Hayashi, M. and Rosenberry, D. O.: Effects of ground water exchange on the hydrology and ecology of surface water, Ground Water, 40, 309–316, 2002.
Hoehn, E. and Cirpka, O. A.: Assessing residence times of hyporheic ground water in two alluvial flood plains of the Southern Alps using water temperature and tracers, Hydrol. Earth Syst. Sci., 10, 553–563, doi:10.5194/hess-10-553-2006, 2006.
Keery, J., Binley, A., Crook, N., and Smith, J. W. N.: Temporal and spatial variability of groundwater-surface water fluxes: Development and application of an analytical method using temperature time series, J. Hydrol., 336, 1–16, doi:10.1016/j.jhydrol.2006.12.003, 2007.
Lagarias, J. C., Reeds, J. A., Wright, M. H., and Wright, P. E.: Convergence properties of the Nelder-Mead simplex method in low dimensions, SIAM J. Optim., 9, 112–147, 1998.
Lautz, L. K.: Impacts of nonideal field conditions on vertical water velocity estimates from streambed temperature time series, Water Resour. Res., 46, W01509, doi:10.1029/2009wr007917, 2010.
Lowry, C. S., Walker, J. F., Hunt, R. J., and Anderson, M. P.: Identifying spatial variability of groundwater discharge in a wetland stream using a distributed temperature sensor, Water Resour. Res., 43(9), W10408, doi:10.1029/2007wr006145, 2007.
Molina-Giraldo, N., Bayer, P., Blum, P., and Cirpka, O. A.: Propagation of Seasonal Temperature Signals into an Aquifer upon Bank Infiltration, Ground Water, no-no, 10.1111/j.1745-6584.2010.00745.x, in press, 2011.
Neilson, B. T., Hatch, C. E., Ban, H., and Tyler, S. W.: Solar radiative heating of fiber-optic cables used to monitor temperatures in water, Water Resour. Res., 46(17), W08540, doi:10.1029/2009wr008354, 2010.
Rau, G. C., Andersen, M. S., McCallum, A. M., and Acworth, R. I.: Analytical methods that use natural heat as a tracer to quantify surface water-groundwater exchange, evaluated using field temperature records, Hydrogeol. J., 18, 1093–1110, doi:10.1007/s10040-010-0586-0, 2010.
Schmidt, C., Bayer-Raich, M., and Schirmer, M.: Characterization of spatial heterogeneity of groundwater-stream water interactions using multiple depth streambed temperature measurements at the reach scale, Hydrol. Earth Syst. Sci., 10, 849–859, doi:10.5194/hess-10-849-2006, 2006.
Schneider, P., Vogt, T., Schirmer, M., Doetsch, J. A., Linde, N., Pasquale, N., Perona, P.,

HESSD
8, 6257–6289, 2011

and Cirpka, O. A.: Towards Improved Instrumentation for Assessing River-1 Groundwater Interactions in a Restored River Corridor, Hydrol. Earth Syst. Sci., accepted, 2011.
Schön, J. H.: Physical Properties of Rocks: Fundamentals and Principles of Petrophysics, second ed. Pergamon, Oxford, 583 pp., 1998.
Selker, J., van de Giesen, N., Westhoff, M., Luxemburg, W., and Parlange, M. B.: Fiber optics opens window on stream dynamics, Geophys. Res. Lett., 33(4), L24401, doi:10.1029/2006gl027979, 2006b.
Selker, J. S., Thevenaz, L., Huwald, H., Mallet, A., Luxemburg, W., de Giesen, N. V., Stejskal, M., Zeman, J., Westhoff, M., and Parlange, M. B.: Distributed fiber-optic temperature sensing for hydrologic systems, Water Resour. Res., 42(8), W12202, doi:10.1029/2006wr005326, 2006a.
Shanafield, M., Hatch, C., and Pohll, G.: Uncertainty in thermal time series analysis estimates of streambed water flux, Water Resour. Res., 47(7), W03504, doi:10.1029/2010wr009574, 2011.
Silliman, S. E., Ramirez, J., and McCabe, R. L.: Quantifying downflow through creek sediments using temperature time-series – One-dimensional solution incorporating measured surface-temperature, J. Hydrol., 167, 99–119, 1995.
Stallman, R. W.: Steady 1-dimensional fluid flow in a semi-infinite porous medium with sinusoidal surface temperature, J. Geophys. Res., 70, 2821–2827, 1965.
Steele-Dunne, S. C., Rutten, M. M., Krzeminska, D. M., Hausner, M., Tyler, S. W., Selker, J., Bogaard, T. A., and de Giesen, N. C. V.: Feasibility of soil moisture estimation using passive distributed temperature sensing, Water Resour. Res., 46, W03534, doi:10.1029/2009wr008272, 2010.
Su, G. W., Jasperse, J., Seymour, D., and Constantz, J.: Estimation of hydraulic conductivity in an alluvial system using temperatures, Ground Water, 42, 890–901, 2004.
Suárez, F., Aravena, J. E., Hausner, M. B., Childress, A. E., and Tyler, S. W.: Assessment of a vertical high-resolution distributed-temperature-sensing system in a shallow thermohaline environment, Hydrol. Earth Syst. Sci., 15, 1081–1093, doi:10.5194/hess-15-1081-2011, 2011.
Taylor, C. J., Pedregal, D. J., Young, P. C., and Tych, W.: Environmental time series analysis and forecasting with the Captain toolbox, Environ. Modell. Softw., 22, 797–814, doi:10.1016/j.envsoft.2006.03.002, 2007.
Tyler, S. W., Selker, J. S., Hausner, M. B., Hatch, C. E., Torgersen, T., Thodal, C. E., and

HESSD
8, 6257–6289, 2011

Schladow, S. G.: Environmental temperature sensing using Raman spectra DTS fiber-optic methods, Water Resour. Res., 45(11), W00D23, doi:10.1029/2008wr007052, 2009.
Vogt, T., Hoehn, E., Schneider, P., and Cirpka, O. A.: Investigation of bank filtration in gravel and sand aquifers using time-series analysis, Grundwasser, 14, 179–194, doi:10.1007/s00767-009-0108-y, 2009.
Vogt, T., Hoehn, E., Schneider, P., Freund, A., Schirmer, M., and Cirpka, O. A.: Fluctuations of electrical conductivity as a natural tracer for bank filtration in a losing stream, Adv. Water Resour., 33, 1296–1308, doi:10.1016/j.advwatres.2010.02.007, 2010a.
Vogt, T., Schneider, P., Hahn-Woernle, L., and Cirpka, O. A.: Estimation of seepage rates in a losing stream by means of fiber-optic high-resolution vertical temperature profiling, J. Hydrol., 380, 154–164, doi:10.1016/j.jhydrol.2009.10.033, 2010b.
Westhoff, M. C., Savenije, H. H. G., Luxemburg, W. M. J ., Stelling, G. S., van de Giesen, N. C., Selker, J. S., Pfister, L., and Uhlenbrook, S.: A distributed stream temperature model using high resolution temperature observations, Hydrol. Earth Syst. Sci., 11, 1469–1480, doi:10.5194/hess-11-1469-2007, 2007.
Young, P. C., Pedregal, D. J., and Tych, W.: Dynamic harmonic regression, Journal of Forecasting, 18, 369–394, 1999.

HESSD
8, 6257–6289, 2011

Table 1. Thermal and hydraulic properties after Schön (1998) and de Marsily (1986) used for analysis and modeling. N and α are the van Genuchten parameters for sandy loam after Carsel and Parrish (1988).

Density of water ($kg\,m^{-3}$)	1000
Density of solids ($kg\,m^{-3}$)	2680
Specific heat capacity of water ($J\,kg^{-1}\,K^{-1}$)	4190
Specific heat capacity of solids ($J\,kg^{-1}\,K^{-1}$)	733
Heat conductivity of water ($W\,m^{-1}\,K^{-1}$)	0.58
Heat conductivity of solids ($W\,m^{-1}\,K^{-1}$)	4.47
Thermal conductivity of gas phase ($W\,m^{-1}\,K^{-1}$)	0.025
Porosity (–)	0.25
Longitudinal dispersivity (m)	0.1
Transverse dispersivity (m)	0.001
Specific discharge of aquifer for uniform flow ($m\,s^{-1}$)	6.9×10^{-5}
Specific discharge of aquifer for depth variable flow ($m\,s^{-1}$)	$5.8–10.4 \times 10^{-5}$
α ($1\,m^{-1}$)	5
N	1.4

HESSD
8, 6257–6289, 2011

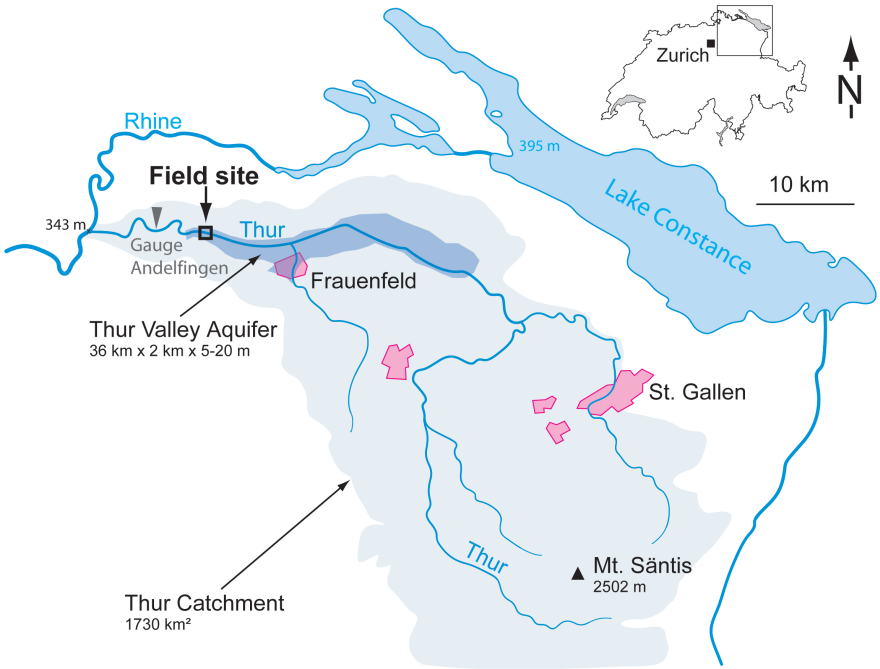

Fig. 1. Thur catchment and location of the field site at the restored river section Niederneunforn/Altikon.

HESSD
8, 6257–6289, 2011

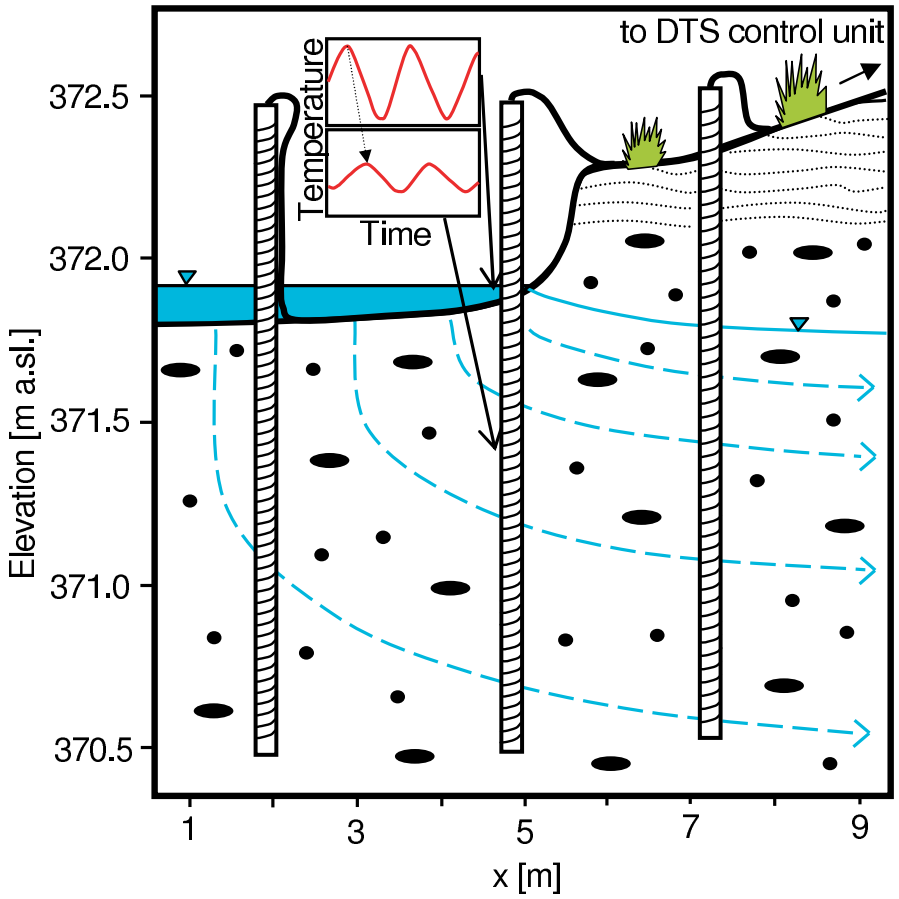

Fig. 2. Sketch of the experimental set-up in the field. During low river stage the top sediments of the fiber-optic high-resolution pole at the shoreline were unsaturated.

HESSD
8, 6257–6289, 2011

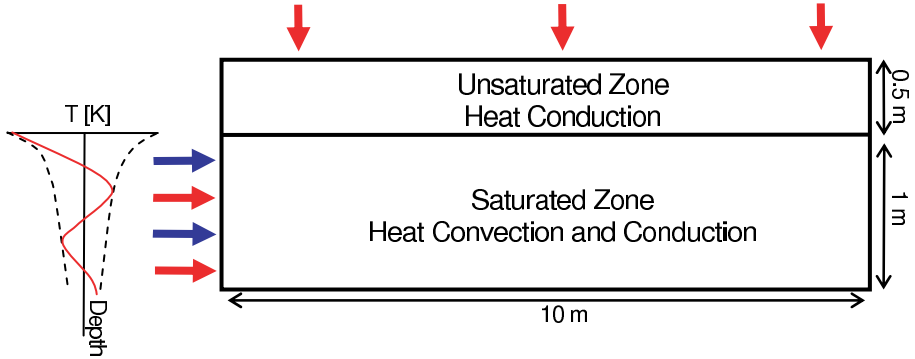

Fig. 3. Set-up of the numerical 2-D heat transport model. Blue arrows indicate horizontal groundwater inflow, red arrows indicate periodic heat input. For the periodic heat input on the left side of the aquifer observed amplitude and time-shift profiles of the high-resolution pole at the shoreline are converted into temperature fluctuations.

HESSD
8, 6257–6289, 2011

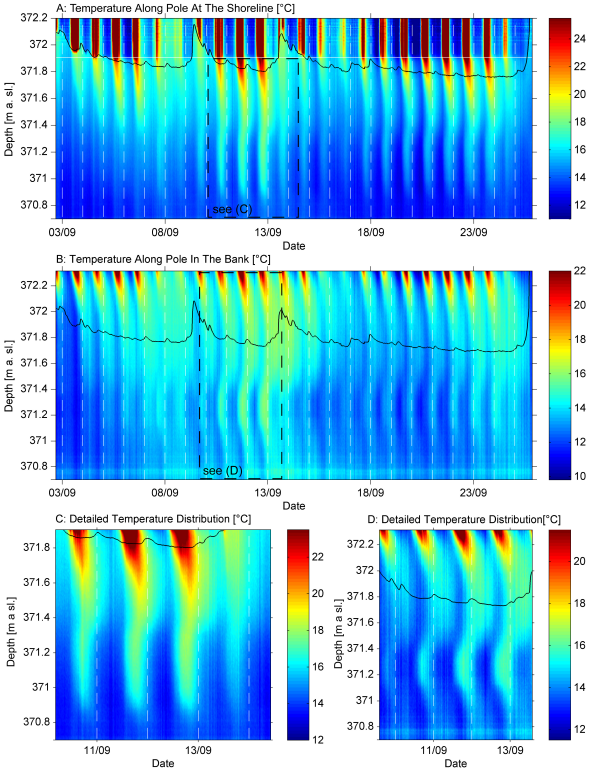

Fig. 4. Temperature distribution along the fiber-optic temperature profilers. The black solid line indicates the water level. **(A)** Shoreline. The white solid line indicates the top of the sediments. The presence of an unsaturated zone depends on the river stage. **(B)** Riparian bank. The top of the figure marks the land surface. During the monitoring period the thickness of the unsaturated zone varied between 0.25–0.60 m. **(C)** Detailed temperature distribution of the sediments at the shoreline. **(D)** Detailed temperature distribution in the riparian bank.

HESSD
8, 6257–6289, 2011

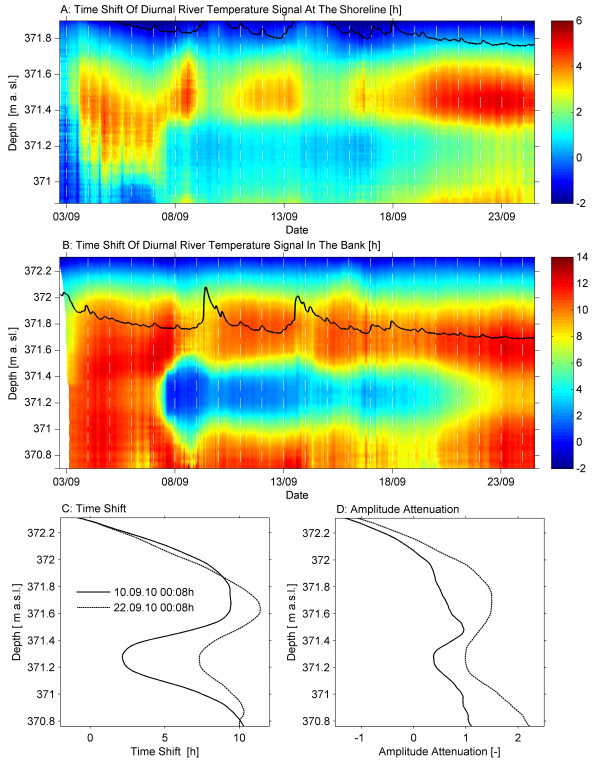

Fig. 5. Results of dynamic harmonic regression **(A)** Time shift of the diurnal river signal over depth and time in the sediments at the shoreline. The black solid line indicates the water level. **(B)** Time shift of the diurnal river signal over depth and time in the riparian bank. The black solid line indicates the water level. **(C)** Temporal and vertical variability of the time shift in the bank as a function of depth during elevated water table (371.9 m a.s.l. on 10 September 2010) and low water table (371.7 m a.s.l. on 22 September 2010). **(D)** Temporal and vertical variability of the amplitude attenuation below groundwater table in the bank as a function of depth during elevated water table (371.9 m a.s.l. on 10 September 2010) and low water table (371.7 m a.s.l. on 22 September 2010).

HESSD
8, 6257–6289, 2011

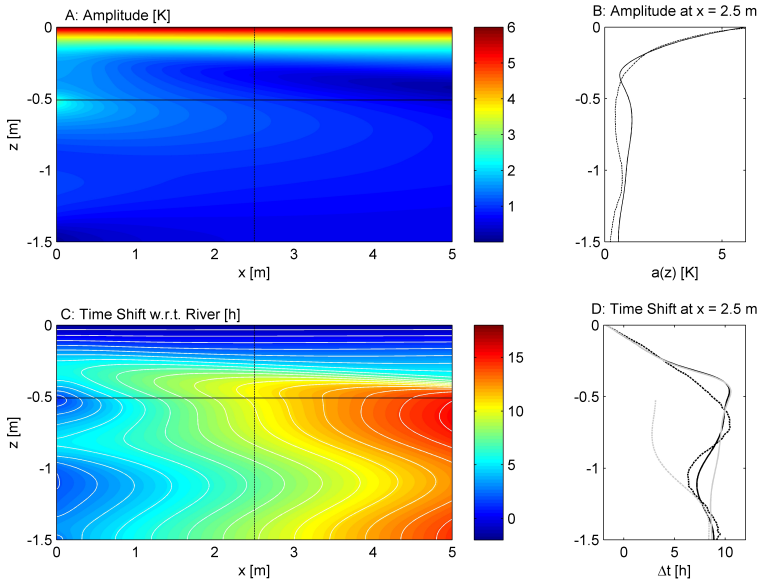

Fig. 6. Modeling results for depth varying horizontal groundwater flow velocity. **(A)** Simulated amplitude of the diurnal temperature signal. The horizontal black solid line indicates water the table and the vertical black dashed line shows the location of the amplitude profile. **(B)** Amplitude profile at 2.5 m distance to the river (black solid line). The black dashed line represents the observed amplitude at the pole in the bank. **(C)** Simulated time shift of the diurnal temperature signal. The horizontal black solid line indicates water table, the vertical black dashed line shows the location of the time-shift profile, and the white lines indicate isochrones of 1 h time shift. **(D)** Time-shift profile at 2.5 m distance to the river (black solid line). The black dashed line represents the observed time-shift at the pole in the bank, the grey dashed line represents a simulation for the groundwater layer without heat exchange with the unsaturated zone, and the grey solid line shows the time-shift profile for uniform horizontal groundwater flow without velocity differences over depth.

HESSD
8, 6257–6289, 2011